

RESEARCH ARTICLE

10.1002/2014JB011697

Key Points:

- Core surface flow with acceleration estimated from geomagnetic data
- Flows predict magnetic field better than Gauss coefficient extrapolation
- Geomagnetic jerks make geomagnetic secular variation forecasting difficult

Correspondence to:

K. A. Whaler,
kathy.whaler@ed.ac.uk

Citation:

Whaler, K. A., and C. D. Beggan (2015), Derivation and use of core surface flows for forecasting secular variation, *J. Geophys. Res. Solid Earth*, 120, 1400–1414, doi:10.1002/2014JB011697.

Received 15 OCT 2014

Accepted 5 FEB 2015

Accepted article online 11 FEB 2015

Published online 18 MAR 2015

Derivation and use of core surface flows for forecasting secular variation

K. A. Whaler¹ and C. D. Beggan²

¹School of GeoSciences, University of Edinburgh, Edinburgh, UK, ²British Geological Survey, Murchison House, Edinburgh, UK

Abstract Improving forecasts of the temporal and spatial changes of the Earth's main magnetic field over periods of less than 5 years has important scientific and economic benefits. Various methods for forecasting the rate of change, or secular variation, have been tried over the past few decades, ranging from the extrapolation of trends in ground observatory measurements to computational geodynamo modeling with data assimilation from historical magnetic field models. We examine the utility of an intermediate approach, using temporally varying core surface flow models derived from relatively short periods of magnetic field data to produce, by advection, secular variation estimates valid for the Earth's surface. We describe a new method to compute a core flow changing linearly with time from magnetic secular variation and acceleration data. We invert a combination of data from the CHAMP satellite mission and ground observatories over the period 2001.0 to 2010.0 for a series of such models. We assess their ability to forecast magnetic field changes by comparing them to CHAOS-4, a state-of-the-art model using data from 1997 to 2014.5. We show that the magnetic field predictions tend to have a lower root-mean-square difference from CHAOS-4 than the International Geomagnetic Reference Field or World Magnetic Map series of secular variation models.

1. Introduction

The Earth's main magnetic field is generated and sustained by dynamo action within the fluid outer core. Although detailed understanding of the processes remains difficult to establish, from ground and satellite observations it is clear that the main field evolves on decadal—as well as many other—timescales.

Forecasting temporal and spatial changes (secular variation or SV) of the Earth's main magnetic field over periods of less than 5 years has important scientific and economic benefits, for example, in areas such as magnetospheric research [e.g., *Shi et al.*, 2014], or providing navigation and orientation capabilities for personal technology devices [e.g., *Wahdan et al.*, 2014]. The primary magnetic field models used for such purposes are the International Geomagnetic Reference Field (IGRF) model issued by the scientific community [*Finlay et al.*, 2010b] and the UK/USA World Magnetic Model (WMM) series [*Maus et al.*, 2010]. Both models provide a predictive element valid for 5 years from the time of release. In the case of the eleventh generation IGRF (IGRF-11) model, the prediction of SV for 2010–2015 was computed from eight different candidate models [*Finlay et al.*, 2010a]. Most of the candidate SV models, such as that of *Hamilton et al.* [2010], were derived from extrapolation of model coefficients using splines or similar mathematical functions, though that of *Kuang et al.* [2010] was the output from a geodynamo assimilation model. Using geodynamo assimilation approaches requires a large volume of data and computational effort [e.g., *Gillet et al.*, 2009; *Fournier et al.*, 2013], while extrapolation is essentially a mathematical technique. Instead, we reexamine a method of intermediate complexity by applying a physics-based method, whereby magnetic field changes are used to infer a large-scale core surface flow with simple temporal variation, which is then used to predict the SV.

Our method assumes that the liquid core has a high electrical conductivity, in which case the principal mechanism for the large-scale change of the magnetic field is advective flow of the liquid outer core; i.e., it satisfies the so-called frozen-flux approximation [*Roberts and Scott*, 1965]. The nature of this fluid motion has been a matter of ongoing research for several decades since *Kahle et al.* [1967] determined flow along the core-mantle boundary (CMB) from measurements of the SV. However, there are severe ambiguities in flows deduced in this manner [*Roberts and Scott*, 1965; *Backus*, 1968], which must be reduced or removed by assuming, for example, tangentially geostrophic [*Hills*, 1979; *Le Mouél*, 1984],

quasi-geostrophic [Pais and Jault, 2008], toroidal-only [Whaler, 1980], or steady [Gubbins, 1982; Voorhies and Backus, 1985] flows, or flows with a particular helicity [Amit and Olson, 2004]. However, the correct recovery of the flow depends on more than having the correct physical assumption. Hence, even with these restrictive assumptions, the detailed CMB flow remains difficult to recover [Rau et al., 2000; Amit et al., 2007; Aubert and Fournier, 2011; Fournier et al., 2011; Aubert, 2013] or may even produce plausible but unphysical configurations [Beggan and Whaler, 2008].

Despite the difficulties of deducing the CMB flow from observations of magnetic field change, they appear to contain some information about the underlying processes. For example, they reproduce decadal timescale changes in length of day associated with angular momentum exchange between the core and mantle from an independent data set [Jault et al., 1988; Holme and de Viron, 2013]. Previous studies have examined the feasibility of forecasting SV advectively by steady core flows, as an alternative to extrapolation of observatory time series or spherical harmonic (Gauss) coefficients describing the main field. Retrospective analysis of such an attempt by Maus et al. [2008] suggested that they could not usefully predict the change of the field over periods longer than a decade. However, this was based on a restrictive choice of flow geometry. Later, Beggan and Whaler [2010] showed that SV forecasting with a steady core flow obtained from magnetic field data in the period 2001–2005 would have improved the accuracy of IGRF-10 at the end of its lifetime. This suggested that short-term forecasting by core flows could be used to produce consistent improvements over extrapolation methods.

A number of temporal phenomena such as geomagnetic jerks [Courillot and Le Mouél, 1984; Brown et al., 2013] cannot be correctly modeled by simple core flow models, as these step changes in the second time derivative of the main field are associated with an acceleration of the flow [Gubbins, 1984; Olsen and Mandea, 2008; Silva and Hulot, 2012]. The appearance and morphology of jerks is still poorly understood, and (as yet) they cannot be predicted. However, with improved magnetic field data coverage from satellite measurements over the decade for geopotential research (2000–2010) and the European Space Agency Swarm mission, it is now feasible to model such higher order changes in the magnetic field [e.g., Rother et al., 2013; Sabaka et al., 2013; Olsen et al., 2014]. In order to capture better these nonlinear events, we have determined core flow models with simple temporal variability and examine their predictive capability.

Our method is much simpler and significantly less costly computationally than geodynamo assimilation methods [e.g., Fournier et al., 2013], in which observations of the field are used to constrain the evolution of a three-dimensional self-consistent geodynamo simulation. However, geodynamo assimilation approaches include both diffusion and advection, whereas methods based on core flow inversion use the frozen-flux approximation. A geodynamo simulation models the magnetic field and flow throughout the core, down to smaller length scales than are deduced from surface observations, and therefore includes the longer wavelength features that can arise from the interaction between small-scale flow and small-scale magnetic field which are missing in flow inversion-based methods [Eymin and Hulot, 2005]. The effect of varying the nondimensional parameters characterizing the system can be investigated, bearing in mind that not all can be assigned Earth-like values in dynamo simulations. Fournier et al. [2011] show that geodynamo data assimilation provides a superior field forecast to linear extrapolation.

In section 2 we outline our method for estimating core flow models consisting of the steady part of the flow and a steady acceleration directly from SV and secular acceleration (SA) data. In section 3, we use a series of flow models based on observatory and satellite data over different epochs in the period 2000–2010 to forecast the SV, taking into account the known occurrence times of jerks. In section 4 we discuss the implications of our results for improving SV forecasts.

2. Method

The inverse problem of deriving a core flow model is typically approached through relating the spherical harmonic representations for the main field (the Gauss coefficients, collected into a vector \mathbf{g}), its first time derivative or SV (coefficients $\dot{\mathbf{g}}$), and the flow (coefficients \mathbf{m}) [e.g., Roberts and Scott, 1965; Holme, 2007]. As the horizontal velocity averages spatially to zero over the core-mantle boundary (CMB) with the radial component at this material boundary vanishing, the flow can be expressed in terms of poloidal (T) and toroidal (S) scalars. Their spherical harmonic coefficients, \mathbf{t} and \mathbf{s} , respectively, collected together into the model vector \mathbf{m} , are the flow model coefficients whose values we seek using a regularized inversion

approach [Gubbins, 1983]. Assuming that the SV is generated by advective flow, the radial component of the induction equation is

$$\dot{B}_r = -B_r \nabla_H \cdot \mathbf{u} - \mathbf{u} \cdot \nabla_H B_r \quad (1)$$

where \dot{B}_r is the time derivative of the radial magnetic field, ∇_H is the horizontal del operator, and \mathbf{u} is the flow velocity.

Maus et al. [2008] additionally included secular acceleration information in their inversion. Differentiating equation (1) gives

$$\ddot{B}_r = -\dot{B}_r \nabla_H \cdot \mathbf{u} - B_r \nabla_H \cdot \dot{\mathbf{u}} - \dot{\mathbf{u}} \cdot \nabla_H B_r - \mathbf{u} \cdot \nabla_H \dot{B}_r \quad (2)$$

where \ddot{B}_r is the second time derivative of the radial magnetic field (expressed through a vector of spherical harmonic coefficients $\dot{\mathbf{g}}$) and $\dot{\mathbf{u}}$ is the flow acceleration. Following Maus et al. [2008], we expand the flow in a Taylor series and retain the first two terms, describing the steady part of the flow and a steady acceleration:

$$\mathbf{u}(t) = \mathbf{u}_0 + (t - t_0)\dot{\mathbf{u}}_0 \quad (3)$$

where $\mathbf{u}_0 = \mathbf{u}(t_0)$ and $\frac{d\mathbf{u}}{dt} = \dot{\mathbf{u}}_0$ are constants. Substituting into equations (1) and (2), we obtain

$$\dot{B}_r = -B_r \nabla_H \cdot (\mathbf{u}_0 + (t - t_0)\dot{\mathbf{u}}_0) - (\mathbf{u}_0 + (t - t_0)\dot{\mathbf{u}}_0) \cdot \nabla_H B_r \quad (4)$$

$$\ddot{B}_r = -\dot{B}_r \nabla_H \cdot (\mathbf{u}_0 + (t - t_0)\dot{\mathbf{u}}_0) - B_r \nabla_H \cdot \dot{\mathbf{u}}_0 - \dot{\mathbf{u}}_0 \cdot \nabla_H B_r - (\mathbf{u}_0 + (t - t_0)\dot{\mathbf{u}}_0) \cdot \nabla_H \dot{B}_r \quad (5)$$

which can be rearranged as

$$\dot{B}_r = -B_r \nabla_H \cdot \mathbf{u}_0 - (t - t_0)B_r \nabla_H \cdot \dot{\mathbf{u}}_0 - \mathbf{u}_0 \cdot \nabla_H B_r - (t - t_0)\dot{\mathbf{u}}_0 \cdot \nabla_H B_r \quad (6)$$

$$\ddot{B}_r = -\dot{B}_r \nabla_H \cdot \mathbf{u}_0 - B_r \nabla_H \cdot \dot{\mathbf{u}}_0 - (t - t_0)\dot{B}_r \nabla_H \cdot \dot{\mathbf{u}}_0 - \dot{\mathbf{u}}_0 \cdot \nabla_H B_r - \mathbf{u}_0 \cdot \nabla_H \dot{B}_r - (t - t_0)\dot{\mathbf{u}}_0 \cdot \nabla_H \dot{B}_r \quad (7)$$

By manipulating equations (6) and (7) in which quantities have been expressed as spherical harmonic expansions, we obtain

$$\dot{\mathbf{g}} = (\mathbf{E}(\mathbf{g}) : \mathbf{G}(\mathbf{g})) \begin{pmatrix} \mathbf{t} \\ \dots \\ \mathbf{s} \end{pmatrix} + (t - t_0)(\mathbf{E}(\mathbf{g}) : \mathbf{G}(\mathbf{g})) \begin{pmatrix} \dot{\mathbf{t}} \\ \dots \\ \dot{\mathbf{s}} \end{pmatrix} = (\mathbf{H} : (t - t_0)\mathbf{H}) \begin{pmatrix} \mathbf{m} \\ \dots \\ \dot{\mathbf{m}} \end{pmatrix} \quad (8)$$

$$\ddot{\mathbf{g}} = (\mathbf{E}(\dot{\mathbf{g}}) : \mathbf{G}(\dot{\mathbf{g}}) : \mathbf{E}(\mathbf{g}) : \mathbf{G}(\mathbf{g})) \begin{pmatrix} \mathbf{t} \\ \dots \\ \mathbf{s} \\ \dots \\ \dot{\mathbf{t}} \\ \dots \\ \dot{\mathbf{s}} \end{pmatrix} + (t - t_0)(\mathbf{E}(\dot{\mathbf{g}}) : \mathbf{G}(\dot{\mathbf{g}})) \begin{pmatrix} \dot{\mathbf{t}} \\ \dots \\ \dot{\mathbf{s}} \end{pmatrix} = (\dot{\mathbf{H}} : (t - t_0)\dot{\mathbf{H}} + \mathbf{H}) \begin{pmatrix} \mathbf{m} \\ \dots \\ \dot{\mathbf{m}} \end{pmatrix} \quad (9)$$

where \mathbf{t} and \mathbf{s} are toroidal and poloidal acceleration coefficient vectors, respectively, and \mathbf{E} and \mathbf{G} are the Elsasser and Gaunt matrices [e.g., Roberts and Scott, 1965; Whaler, 1986]. The Elsasser and Gaunt matrix elements are functions of either the main field or SV coefficients, as indicated by the quantity in parentheses. The combined Elsasser and Gaunt matrices are denoted \mathbf{H} and $\dot{\mathbf{H}}$, and the steady flow and acceleration model coefficient vectors are denoted \mathbf{m} and $\dot{\mathbf{m}}$, respectively.

Most previous flow inversions have treated spherical harmonic coefficients of the SV (or SV and SA) as data and solved equation (8) (or (8) and (9)) for the flow. However, $\dot{\mathbf{g}}$ and $\ddot{\mathbf{g}}$ are linearly related to orthogonal component SV (and SA) data on (or near) the surface of the Earth, e.g., we can write $\dot{\mathbf{d}} = \mathbf{Y}\dot{\mathbf{g}}$. Hence, our data are magnetic field observations, arranged in vectors $\dot{\mathbf{d}}$ and $\ddot{\mathbf{d}}$. The elements of $\dot{\mathbf{d}}$ are the components of the observed SV (here \dot{X} , \dot{Y} , and \dot{Z} , the north, east, and vertically downward components, respectively) expressed in spherical polar coordinates (r , θ , ϕ). \mathbf{Y} has elements which are multiples of spherical harmonics

and their θ and ϕ derivatives. A similar expression, $\dot{\mathbf{d}} = \mathbf{Y}\dot{\mathbf{g}}$, applies to the SA. We substitute these expressions into equations (8) and (9) to give

$$\dot{\mathbf{d}} = \mathbf{Y}(\mathbf{H} : (t - t_0)\mathbf{H}) \begin{pmatrix} \mathbf{m} \\ \dots \\ \dot{\mathbf{m}} \end{pmatrix} = (\mathbf{A} : (t - t_0)\mathbf{A}) \begin{pmatrix} \mathbf{m} \\ \dots \\ \dot{\mathbf{m}} \end{pmatrix} \quad (10)$$

$$\ddot{\mathbf{d}} = \mathbf{Y}(\dot{\mathbf{H}} : (t - t_0)\dot{\mathbf{H}} + \mathbf{H}) \begin{pmatrix} \mathbf{m} \\ \dots \\ \dot{\mathbf{m}} \end{pmatrix} = (\dot{\mathbf{A}} : (t - t_0)\dot{\mathbf{A}} + \mathbf{A}) \begin{pmatrix} \mathbf{m} \\ \dots \\ \dot{\mathbf{m}} \end{pmatrix} \quad (11)$$

where $\mathbf{A} = \mathbf{YH}$ and $\dot{\mathbf{A}} = \mathbf{Y}\dot{\mathbf{H}}$. This provides a pair of coupled linear equations relating SV and SA observations to coefficients of the steady part of the flow and its steady acceleration, hereafter loosely referred to as a steady flow and acceleration model.

We illustrate the solution method on the inversion for just a steady flow; the extension to steady flow and acceleration is straightforward. *Gubbins* [1983] pioneered the application of regularized inversion in geomagnetism, in which an objective function, measuring a combination of the fit to the data and the smoothness of the solution, is minimized. The inclusion of this additional regularization term leads to a model $\hat{\mathbf{m}}$ given by

$$\hat{\mathbf{m}} = (\mathbf{A}^T \mathbf{C}^{-1} \mathbf{A} + \lambda \mathbf{D})^{-1} \mathbf{A}^T \mathbf{C}^{-1} \mathbf{d} \quad (12)$$

\mathbf{C} is the data covariance matrix, here assumed diagonal, and \mathbf{D} is the regularization matrix which can be used to incorporate an a priori constraint on the flow, imposing "smoothness." The \mathbf{A} matrix contains the equations of condition for each observation. A damping parameter, λ , acts to control the importance attached to fitting the data versus the imposition of a smooth flow. Regularization also ensures numerical stability of the inversion and convergence of the truncated spherical harmonic series for $\hat{\mathbf{m}}$. In this study, we use the "strong norm" of *Bloxham* [1988] to minimize a global measure of the flow complexity:

$$\begin{aligned} \mathbf{m}^T \mathbf{D} \mathbf{m} &= \oint_{\text{CMB}} [(\nabla_h^2 u_\theta)^2 + (\nabla_h^2 u_\phi)^2] dS \\ &= 4\pi \sum_l \frac{[l(l+1)]^3}{2l+1} \sum_{m=0}^l [(t_l^m)^2 + (s_l^m)^2] \end{aligned} \quad (13)$$

Since we combine data from more than three epochs, the steady part of the flow is uniquely determined [*Voorhies and Backus*, 1985] and, by extension, also the steady part of the acceleration. We do not make any other assumptions about the form of the flow.

Walker and Jackson [2000] provide the motivation to calculate the model by an iterative one-norm minimization method. In particular, they offer empirical evidence that the distribution of residuals from a historical magnetic dataset comprising vector, scalar, and directional data is well described by a double-Laplacian probability distribution. Similarly, *Beggan and Whaler* [2008] and *Beggan et al.* [2009] found Laplacian distributed SV residuals, when modeled by a core surface flow.

The formulation of the one-norm solution follows the method set out by *Walker and Jackson* [2000]. The residual errors from the previous iteration are used to generate an additional diagonal matrix \mathbf{R} , whose elements are $R_{ij} = \sqrt{2}/|e_i|$, where e_i is the residual of the i th datum. As \mathbf{R} is calculated at each iteration, k , the data are iteratively reweighted, reducing the influence of outliers. For a diagonal data covariance matrix, as assumed here, the iterative one-norm solution can be written as

$$\hat{\mathbf{m}}_{k+1} = (\mathbf{A}^T \sqrt{\mathbf{C}^{-1}} \mathbf{R}_k \sqrt{\mathbf{C}} \mathbf{A} + \lambda \mathbf{D})^{-1} (\mathbf{A}^T \sqrt{\mathbf{C}^{-1}} \mathbf{R}_k \sqrt{\mathbf{C}} \mathbf{d}). \quad (14)$$

We use a two-norm solution as the initial guess for $\hat{\mathbf{m}}$, compute the residuals between the data (here magnetic field observations) and the model as $\mathbf{e} = \mathbf{d} - \mathbf{A}\hat{\mathbf{m}}$, update \mathbf{R} accordingly, and then iterate until the sum of the absolute values of the difference between the data and the model predictions converges.

We point out that our approach differs from that of *Maus et al.* [2008] in several aspects. As already noted, it is based on one-norm minimization, and on inverting SV and SA data directly rather than spherical

harmonic models of them. *Maus et al.* [2008] calculated the Gaunt and Elsasser matrices numerically, whereas we use analytic expressions for them. They inverted for just zonal toroidal flow acceleration coefficients, with the same truncation level and damping parameter as for the flow. We truncated the spherical harmonic expansion of the acceleration at a lower degree ($l=8$) than the flow ($l=14$), reflecting the former's poorer resolution. However, we allow all acceleration coefficients, both toroidal and poloidal, up to the specified truncation level. We also specify different damping parameters for the flow and acceleration part of the model. After investigation, we found that an acceleration damping parameter typically 3 orders of magnitude larger than for the flow led to well-converged, large-scale solutions for both sets of parameters.

To perform a forecast, we advect the main field forward using a time step $\Delta t=0.0833$ years (i.e., 1 month) in an iterative fashion. At the current epoch, k , we insert the main field coefficients $\mathbf{g}_{(k)}$ into the matrix $\mathbf{H}_{(k)}$ to predict the SV spherical harmonic coefficients, $\dot{\mathbf{g}}_{(k)}$, using equation (8). These coefficients are then used in $\dot{\mathbf{H}}_{(k)}$ to predict the SA spherical harmonic coefficients, $\ddot{\mathbf{g}}_{(k)}$, using equation (9). Finally, we forecast the main field Gauss coefficients at epoch $(k+1)$:

$$\mathbf{g}_{(k+1)} = \mathbf{g}_{(k)} + \Delta t \left(\dot{\mathbf{g}}_{(k)} + \frac{\Delta t}{2} (\ddot{\mathbf{g}}_{(k)}) \right) \quad (15)$$

Since the forecast involves both SV and SA, and $\mathbf{H}_{(k)}$ and $\dot{\mathbf{H}}_{(k)}$ are updated each month, it is slightly nonlinear. Hindcasting is undertaken in the same fashion, with a sign change.

3. Steady Flow and Acceleration Models

3.1. Magnetic Field Data

We used two different sets of magnetic field data covering the period 2000–2010 to generate SV and SA estimates. The first was vector monthly mean values based on nighttime data from up to 160 global magnetic observatories, about 2% of which were missing in any given month. As this network is very unevenly spatially distributed, we also used satellite data to provide global coverage. Following the method of *Mandea and Olsen* [2006], we calculated “virtual observatory” (VO) monthly field component time series from CHAMP vector data (version 51) on a grid of 648 points at equal latitude and longitude spacings of 10° , from 5° to 175° in colatitude and 0° to 350° in longitude. Each VO was located at a nominal altitude of 400 km and encompassed satellite data within a 400 km radius from the center point. The VO method compensates for the slow decrease in the orbital altitude over the lifetime of the CHAMP mission. We used the CHAOS-3 model [*Olsen et al.*, 2010] to remove an estimate of the main field before the inversion for the VO solutions, though this does not have any impact on the SV or SA calculated.

Annual first differences of main field and SV values provided SV and SA estimates, respectively, at both ground observatories and VOs. The difference between month $n+12$ and month n was designated to be the value at month $n+6$, giving time series of SV from 2001.875 to 2010.125 and of SA from 2002.375 to 2009.625. Hence, over the time span of interest, there are months at the beginning and end which have only SV data. When the model covered the start and/or the end of our time span, we included SV data even though there were no accompanying SA data.

From the VO method, the variance of each monthly solution for the individual magnetic field components (and hence the SV and SA values derived from them) can be computed. The uncertainties of the ground observatory SV and SA data are unknown but assumed to be small. We assigned them arbitrary values of 1 nT/yr and 1 nT/yr² in each component. We note, though, that the iterative reweighting in the one-norm inversion algorithm should determine an acceptable balance between fitting the ground and satellite data, even if the relative uncertainties on the two data types are not correctly chosen to start with. By assuming a diagonal data covariance matrix, we treat all the data as independent. However, we recognize that SV estimates a year apart have a main field datum in common, and the SA estimates are derived from the SV and so have quite complex data interdependencies.

3.2. Generating Core Flow Models

The Taylor series expansion (equation (3)) was performed about a time approximately in the center of each epoch over which we assumed that the flow and acceleration were steady, but we have also verified that the solution is not sensitive to this choice. There are several proposed geomagnetic jerks in the time period

Table 1. Mean Flow Velocity (km/yr) and Acceleration (km/yr²) for Each Epoch

Model	Flow Velocity	Acceleration
2001–2010	22.1	0.80
2001–2005	11.8	0.57
2001–2007	14.6	0.61
2005–2010	16.8	0.85
2007–2010	14.0	1.06
2003–2005	14.7	0.65

of our data. The most widely recognized are the 2003 jerk [Olsen and Manda, 2007; Wardinski et al., 2008; Silva and Hulot, 2012] and the 2007 jerk [e.g., Olsen et al., 2009; Brown et al., 2013]. We chose to estimate flow models over six time spans of variable length, given in Table 1, to examine the effects of including or excluding data across jerks, and the length of time over which steadiness was assumed.

Damping parameters of 10^{-4} and 0.1 for the flow and acceleration part of the solution gave good results, independent of the number of months included in the inversion and whether they were based on just the ground observatory data or included satellite VO data. The results presented here are all of joint inversions of ground observatory and VO data. The solutions converged after typically fewer than 20 iterations from the two-norm starting model. The main features of the steady part of the flow are common to all our models, but the acceleration changes markedly depending on how many and which months are included in the inversion, possibly reflecting a change in the geometry of the flow when geomagnetic jerks occur. As an example, Figure 1 shows the steady part of the flow (top row) and acceleration (bottom row) of the models for 2001–2007 and 2007–2010 from SV and SA magnetic field data. Prominent features include the band of westward flow straddling the equator between about 90°E and 45°W, particularly in the Southern Hemisphere, slower flow beneath the Pacific Ocean, and an anticlockwise eddy beneath the southern Indian Ocean. The equatorial asymmetry is also seen in the unconstrained flows of Amit and Pais [2013] but is in contrast to flows obtained with the quasi-geostrophic constraint, which imposes equatorial symmetry outside the tangent cylinder [Pais and Jault, 2008; Gillet et al., 2009], and the geodynamo flows of Aubert [2013]. Tangentially geostrophic flows tend to have faster flow in the Pacific hemisphere [e.g., Amit and Pais, 2013]. Table 1 summarizes the mean flow speed and acceleration for each of the periods considered.

The fit to the data was poorer for SA than SV data and for VO than ground observatory data, both as expected. There are large outliers, particularly in the SA data. The spatial data residuals are severely biased, both for ground observatory and VO data, regardless of whether two- or one-norm minimization was performed, as illustrated in Figure 2. Spatial patterns in the residuals to VO SV data were first identified by Beggan et al. [2009] and can be attributed primarily to external field contamination [Shore, 2013]. External

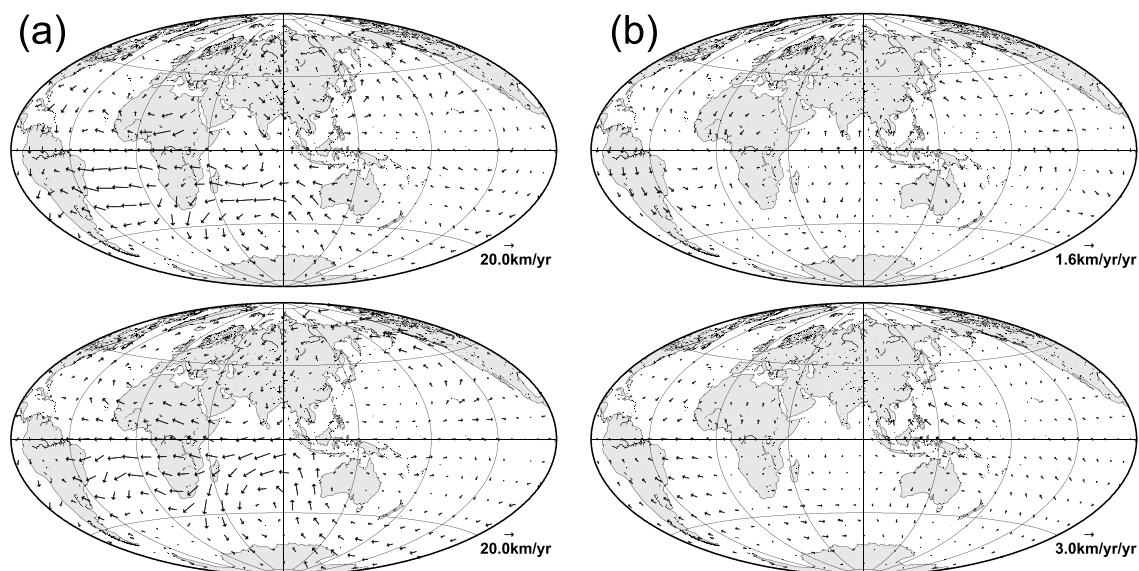


Figure 1. Example of (a) steady core flow and (b) steady acceleration part of two models using data covering the periods (top row) 2001–2007 and (bottom row) 2007–2010. Note the difference in reference arrow value for the acceleration plots.

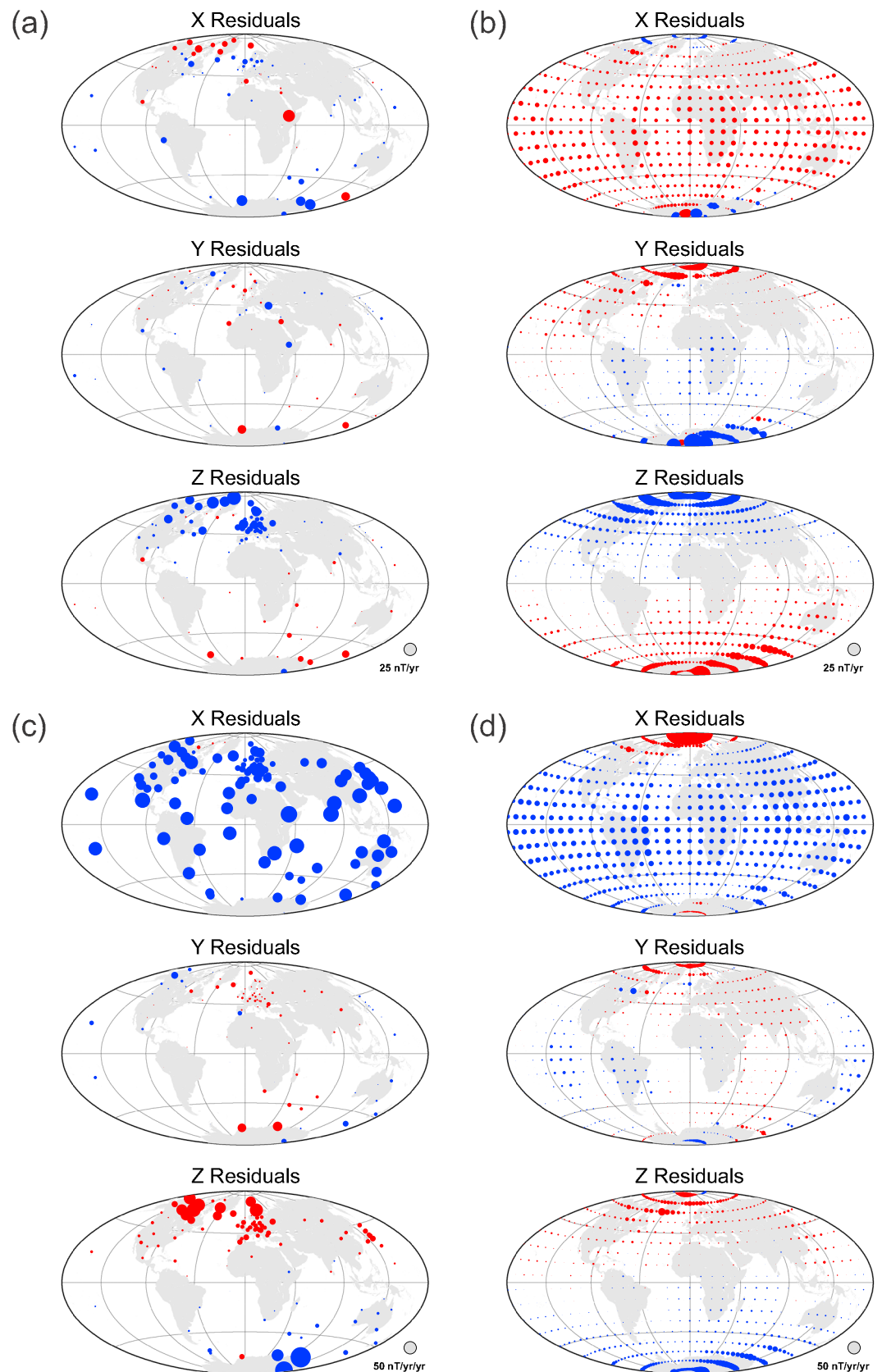


Figure 2. Residuals to (a) ground and (b) VO SV data and (c) ground and (d) VO SA data at 2004.375 for the model covering the period 2001–2005. Red and blue indicate positive and negative residuals, respectively.

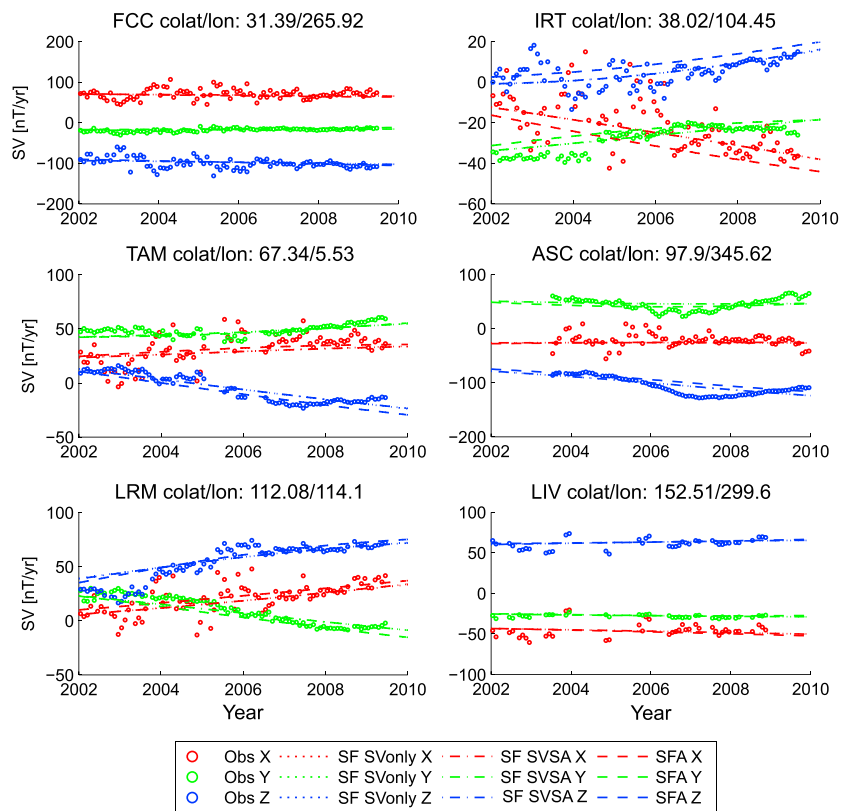


Figure 3. Comparison of measured and predicted SV for six observatories from steady flow models covering the period 2001–2005. Circles denote the data. Dotted lines are predictions by steady flows calculated from SV data only (SF SVOnly), dash-dotted lines by steady flows calculated from SV and SA data (SF SVSA), and dashed lines by steady flow and acceleration models (SFA).

field contamination is also likely to be the cause of the large outliers near the poles, especially in the VO data. The large-scale patterns in the residuals tend to be common to both ground observatory and VO data fits, suggesting that the ground data also have significant external field contamination.

We also produced a series of steady core flow models covering the same date ranges, with the same regularization and damping parameter. One set used only SV data, similar to the technique of *Beggan and Whaler* [2010]; the other set used both SV and SA data (i.e., a joint inversion of equations (10) and (11) with \mathbf{m} set to zero). These will be useful to help determine whether the additional complexity of core acceleration is worthwhile as a predictive tool. Figure 3 shows time series of observatory data annual first differences and their predictions by the three types of flow models. All are able to reproduce the average change in the SV, with an offset between the predictions of steady flows and those with acceleration. Over a longer period than investigated here, we would see greater and more complex differences between the predictions of the three types of flow. The addition of a simple flow acceleration does not allow the model to follow the trends in the data better, e.g., the dip in the vertical component at Ascension Island (ASC) around 2007.

3.3. Forecast and Hindcast Performance

We now wish to determine how well each steady flow and acceleration model performs when forecast or hindcast over part or all of the period 2000.0 to 2014.5 and whether such models perform better than steady flow advection or models in which field coefficients are linearly extrapolated using an estimate of the SV. We have chosen CHAOS-4+ version 3 (<http://www.spacecenter.dk/files/magnetic-models/CHAOS-4/>), released June 2014, as the “true” field model representing the detailed variation of the main field over the time span. CHAOS-4+ version 3 (hereafter CHAOS-4+) is an updated version of the CHAOS-4 model [Olsen et al., 2014] which includes magnetic satellite data from CHAMP, Ørsted, and SAC-C as well as Swarm data

Table 2. Root-Mean-Square Difference (in nT) Between CHAOS-4+ and Six Steady Flow and Acceleration (SFA) Models, Steady Flow Models Using SV and SA Data (SF SVSA), and Steady Flow Models Using SV only (SF SVonly) at the End of the Forecast Periods of 2005–2010 and 2010–2014.5^a

Model	2005–2010			2010–2014.5		
	SF SVonly	SF SVSA	SFA	SF SVonly	SF SVSA	SFA
2001–2005	64	60	65	-	-	-
2003–2005	51	68	68	-	-	-
2001–2007	53	53	37	99	98	98
2001–2010	61	54	34	73	97	93
2005–2010	48	50	20	69	68	73
2007–2010	43	54	49	65	63	63

^aItalicized cells indicate models with data partially covering the forecast period.

[Friis-Christensen et al., 2006] up to the beginning of June 2014 and observatory data throughout. The model consists of Gauss coefficients of the main field up to degree and order 20 between 1997 and 2014.5, which vary temporally according to a sixth-order spline, with 6 month spacing between knot points.

To quantify the difference between the Gauss coefficients of CHAOS-4+ and a forecast or hindcast model, the mean square power of their differences is calculated:

$$dP = \sum_{l=1}^{l_{\max}} \sum_{m=0}^l (l+1) [g_l^m_{\text{actual}} - g_l^m_{\text{model}}]^2 \tag{16}$$

\sqrt{dP} is referred to as the root-mean-square (RMS) difference between the CHAOS-4+ and the forecast or hindcast model and is calculated on a month-by-month basis. This same measure is used for forecasts and hindcasts both using our flow models and a series of International Geomagnetic Reference Field (IGRF) models and World Magnetic Models (WMM). Forecasts/hindcasts by flow advection start at 2000, 2005, or 2010 to match the start dates of successive IGRF and WMM forecasts. The RMS differences for various time intervals of forecast and hindcast are presented in Tables 2 and 3 for flow advection and linear extrapolation, respectively. In the remainder of this section, we examine these RMS differences in more detail and how they accumulate over time.

The dotted lines in Figure 4 show the RMS differences at each month over the period 2000.0–2014.5 for IGRF-9, IGRF-10, IGRF-11, WMM2000, WMM2005, and WMM2010. The IGRF models have a slightly lower difference than the WMMs at the end of each 5 year period. For reference, the retrospective main field estimate from IGRF-11 is shown (red solid line) to illustrate the greater temporal structure of CHAOS-4+ compared to the simple linear evolution of the IGRF models. Note that the models do not wholly agree at the 2000, 2005, and 2010 points, as they use different data selection and modeling techniques. In fact, they disagree by typically 5 nT, so if our flow forecasts and hindcasts have \sqrt{dP} values that differ by less than this, we do not regard them as significantly different in what follows.

Figure 5 shows the RMS differences over 2000.0 to 2014.5 from flow advection forecasts/hindcasts using CHAOS-4+ at 2010.0 as the starting point. Figure 5 (top) is for steady flow models obtained by inversion of SV data only. The model using data from 2007 to 2010 (pale blue solid line) produces the smallest RMS difference from CHAOS-4+ by 2014.5 (65 nT), but those for the 2005–2010 model (green dotted line; 69 nT) and 2001–2010 model (black dashed line; 73 nT) are only marginally larger. For reference, the IGRF-11 RMS difference at 2014.5 is 73 nT (cf.

Table 3. Root-Mean-Square Difference (in nT) Between CHAOS-4+ and SV Forecast of the Contemporaneous IGRF and WMM Models at the End of the Forecast Periods of 2005–2010 and 2010–2014.5

Model	2005–2010	2010–2014.5
IGRF-10/IGRF-11	109	73
WMM2005/WMM2010	122	91

Table 3). Figure 5 (middle) shows the results of using steady flows obtained by inverting both SV and SA data, and the results are indistinguishable to within the estimated uncertainties. Figure 5 (bottom) shows that using the steady flow and acceleration

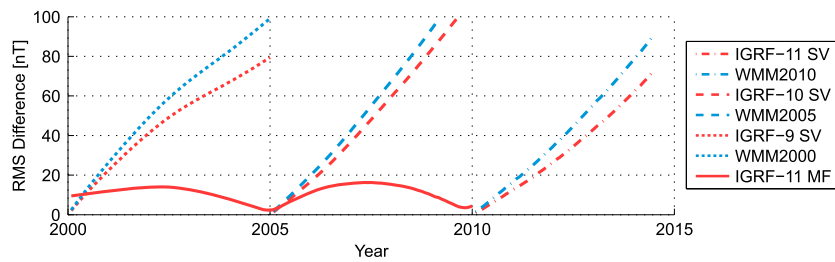


Figure 4. Root-mean-square difference between CHAOS-4+ and the IGRF and WMM model series SV forecasts over the period 2000.0–2014.5. Also shown is the difference between the retrospective main field of the IGRF-11 model (red solid line).

models does not improve the forecast in this case, with the 2005–2010 and 2001–2010 forecasts significantly poorer.

All models perform better at hindcasting than forecasting (as they include data over the period of hindcasting), the difference being particularly pronounced for the 2001–2007 and 2001–2010 models. Hindcasting also reveals the superiority of steady flow and accelerations models. The hindcasts of the 2001–2007 and 2001–2010 models have the smallest differences after 10 years, particularly the former (blue dash-dotted line), presumably as it does not include data encompassing the 2007 jerk. This suggests that capturing temporal variability in the flow is important—so long as the interval does not encompass a jerk, which can strongly affect the flow.

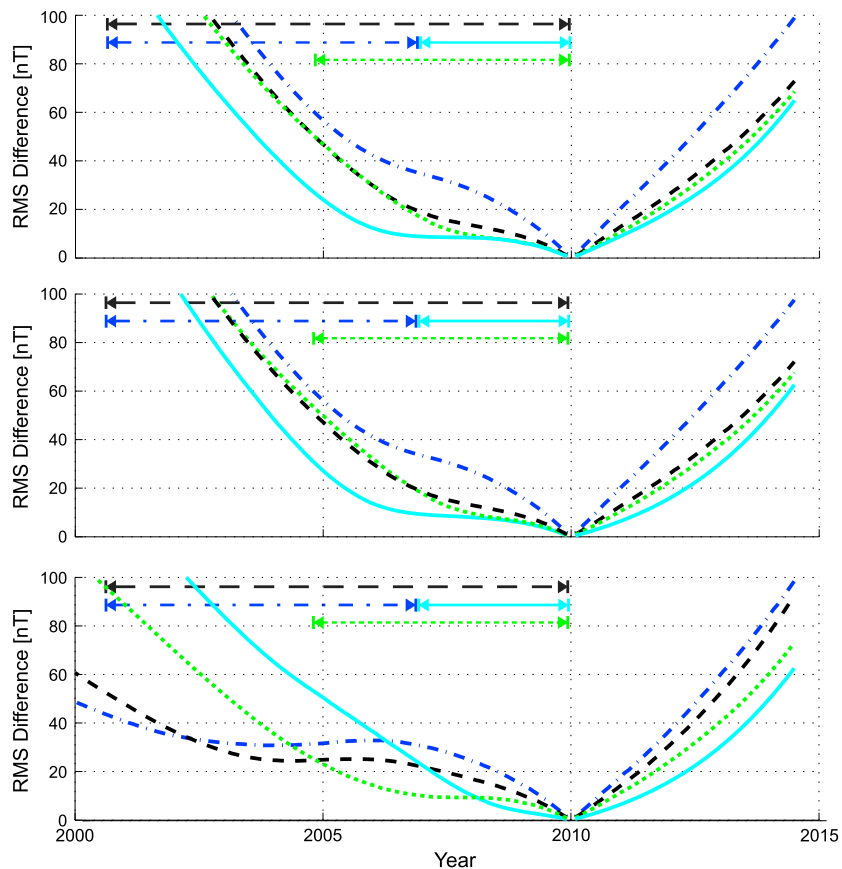


Figure 5. Root-mean-square difference between CHAOS-4+ and forecasts/hindcasts over the period 2000.0–2014.5, starting at 2010.0. (top) Steady flow models inverted using magnetic SV only; (middle) steady flow models inverted using magnetic SV and SA data; and (bottom) steady flow and acceleration models. The horizontal arrows with the same line style and color indicate the data span of each model used.

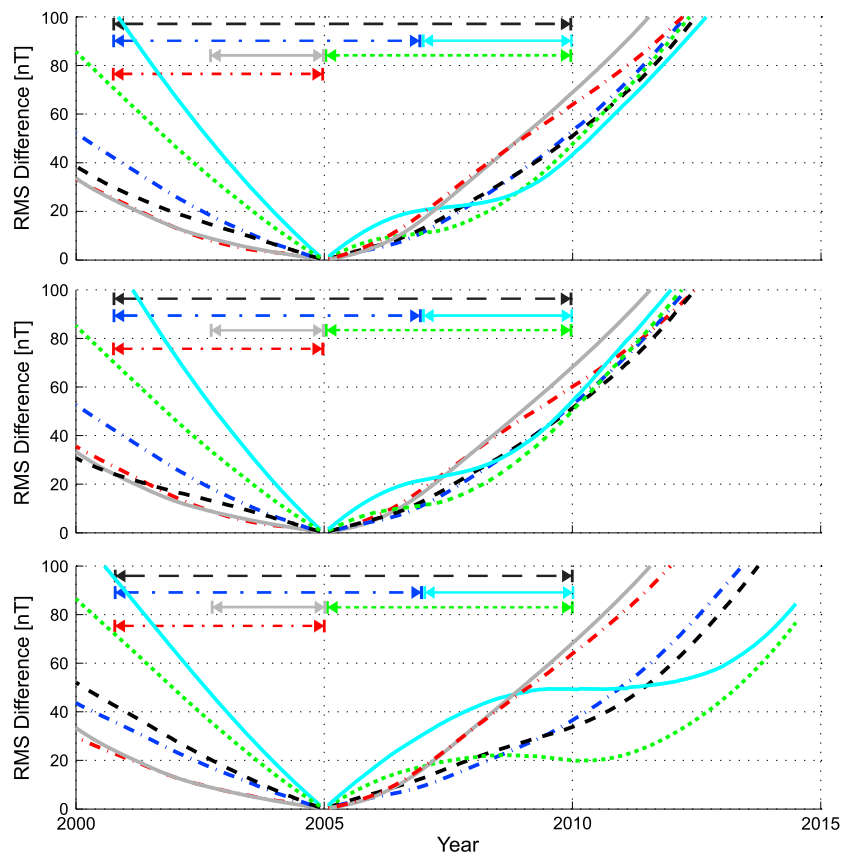


Figure 6. Root-mean-square difference between CHAOS-4+ and forecasts/hindcasts over the period 2000.0–2014.5, starting at 2005.0. (top) Steady flow models inverted using magnetic SV only; (middle) steady flow models inverted using magnetic SV and SA data; and (bottom) steady flow and acceleration models. The horizontal arrows with the same line style and color indicate the data span of each model used.

Figure 6 shows the forecasts and hindcasts starting at 2005.0 rather than 2010.0. The plots are laid out in a similar manner to those in Figure 5. The RMS differences of the forecasts to 2010.0 from the 2001–2005 steady flow models (red dash-dotted line) are indistinguishable, i.e., again there is no obvious advantage to adding a constant flow acceleration in this case.

The steady flow and acceleration forecast of the 2007–2010 model (pale blue solid line) is poor over the period of 2005 to 2010 but does not deteriorate much further between 2010 and 2014.5. Unsurprisingly, the 2005–2010 model (green dotted line) performs best over the 2005–2010 period but also does better over 2010–2014.5 than the 2007–2010 model (RMS differences of 77 nT compared to 85 nT). In contrast to when the start time is 2010.0, the 2001–2010 model (black dashed line) is better at forecasting than hindcasting: 37 nT at 2010.0 versus 51 nT at 2000.0.

The RMS differences of the hindcasts at 2000.0 of the three types of flow model with data from 2005–2010 (green dotted lines) are all similar at approximately 85 nT. The hindcasts from the steady flow and acceleration models do not have much smaller differences than those from steady-flow-only models for 2001–2005 or 2001–2007, while the 2001–2010 steady flow and acceleration model has a larger RMS difference at 2000.0 than that of the steady flows (i.e., 50 nT versus $\lesssim 40$ nT).

Figure 7 shows the forecasts starting from 2000.0, arranged the same way as previously. There are just four flow models, as it is not appropriate to forecast from 2000.0 using data from 5 or 7 years in the future. For models derived from data covering 2001–2007 (blue dash-dotted line) and 2001–2010 (black dashed line), the steady flow forecasts (Figure 7, top and middle) are significantly worse (RMS differences greater than 100 nT after 7 years) than forecasts of steady flow and acceleration (Figure 7, bottom).

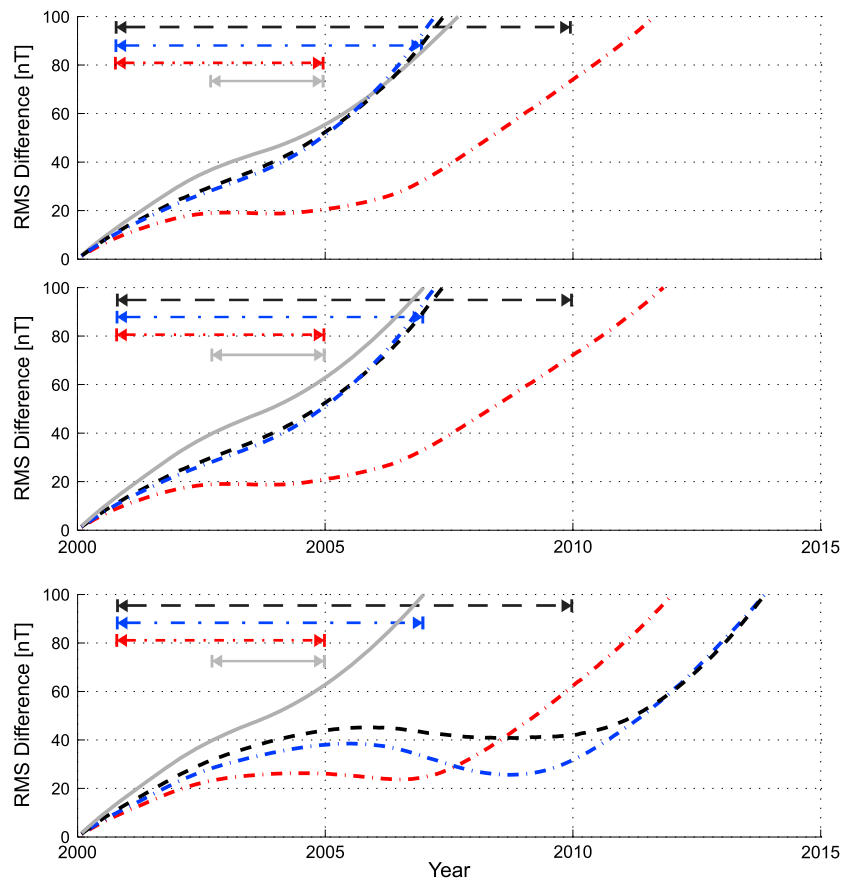


Figure 7. Root-mean-square difference between CHAOS-4+ and forecasts/hindcasts over the period 2000.0–2014.5, starting at 2000.0. (top) Steady flow models inverted using magnetic SV only; (middle) steady flow models inverted using magnetic SV and SA data; and (bottom) steady flow and acceleration models. The horizontal arrows with the same line style and color indicate the data span of each model used.

RMS differences for both steady flow models for 2001–2005 (red dash-dotted line) behave similarly, rising quickly to around 20 nT, plateauing for a few years, and then rising from 2005 onward. The steady flow and acceleration model differences follow a similar pattern but plateau for a longer period. By 2010.0, the difference is 62 nT, the same as its value when the forecast starts at 2005.0 (compare the red dash-dotted lines in Figures 6 (bottom) and 7 (bottom)). This would suggest that, for this case, a longer forecast period is required for the acceleration to have an effect.

The 2003–2005 flow models forecast similar RMS differences, independent of the flow type (gray lines). The steady flow model forecast obtained from SV data only closely follows those of the 2001–2007 and 2001–2010 models. As they do not include data for 2000–2003, none of the model forecasts are particularly good at capturing the changes of the magnetic field in this period.

Comparing Tables 2 and 3, it can be seen that in 2010.0, the forecast from all three flow model types is smaller, typically by a factor 2, than the respective forecast of the IGRF or WMM models, irrespective of the time interval the model covers. It thus would have been highly advantageous to use a core flow model to forecast SV. For the current truly predictive parts (2010–2014.5), all models derived from the 2005–2010 and 2007–2010 data provide RMS differences significantly smaller than both the IGRF and WMM models, as does the steady flow model from SV data only for 2001–2010.

4. Discussion

Our results allow us to assess whether flow models in which acceleration either of the field or the flow are included give a better forecast than simple linear extrapolation of the Gauss coefficients. The additional

computational overhead is small on contemporary computers, but there is little point in adding complexity if it does not yield worthwhile improvements or even makes the forecast worse. The results in Figures 5–7 show that flow advection offers improvements over estimating SV by linear extrapolation but requires care in implementation. Forecast and hindcast ability is usually different, with the differences generally more obvious for steady flow and acceleration models, especially over longer periods when their additional nonlinearities have more effect. For example, the 2001–2007 model (blue dash-dotted line) has an RMS difference of 32 nT at 2010.0 when forecast from 2000.0 (Figure 7) but 49 nT at 2000.0 when hindcast from 2010.0 (Figure 5). The asymmetry varies with start date and flow type. Some steady flow and acceleration models have predicted RMS difference time series that plateau, and even occasionally decrease, for a while, in which case they provide a significantly improved prediction. However, there is no reliable indicator of the combination of data periods used to calculate the model, start date, whether to forecast or hindcast, and over which period that will allow us to take advantage of this behavior. We note that, when they occur, the plateau periods typically coincide with jerk times, although this may be a coincidence.

While flow acceleration improves hindcasts from 2010.0 (but not forecasts) and forecasts from 2000.0 when the models are calculated from data over long periods (Figures 5 and 7), the picture when the start date is 2005.0 (Figure 6) is more complicated because of the jerks that occur either side of this date. *Chulliat et al.* [2010] present evidence that the radial component SA associated with the jerks in 2003 and 2007 was anticorrelated, with slightly lower amplitude in 2003. This suggests that the flow accelerations would also cancel out over the decade, and so a steady flow and acceleration model encompassing both jerks should produce a better forecast than one including only one of them. Therefore, it is surprising that such a model of data from just 2001 to 2007 hindcasts better from 2010.0 to 2000.0, and forecasts better from 2000.0 to 2010.0, than the one based on data from 2001 to 2010 (Figures 5 and 7, respectively). Possibly, the 2007 jerk had a larger effect on the flow acceleration than the 2003 jerk owing to its higher amplitude [*Chulliat et al.*, 2010], and so it affects the 2007–2010 period more; hence, using a model that does not include data reflecting the flow acceleration arising from the 2007 jerk may allow the average change of the field to be followed better over the period 2010.0 to 2000.0.

There are occasions when starting a forecast further back in time using a steady flow and acceleration model can lead to a similar, or even a smaller, RMS difference at the end of the forecast period. For example, the 2005–2010 model forecasts a similar difference at 2014.5, ~75 nT, when commencing the forecast either at 2010.0 or 2005.0, whereas both the 2001–2010 and 2001–2007 models forecast lower values when the forecast begins in 2005.0, ~115 nT, than when the start date is 2010.0, ~125 nT (Figures 5 and 6, respectively). However, only the 2005–2010 model forecasts are improvements over the IGRF and WMM 5 year linear extrapolations.

When forecasting from the end of the time span covered by the data, i.e., from 2010.0 to 2014.5, the earlier the start date of the data that goes into the model, the worse the forecast (Figure 5 and Table 2). The three types of flow model forecast with a similar RMS difference, except for the models based on data from 2001 to 2010 when the flow including acceleration performs noticeably worse. The 2001–2007 models (blue dash-dotted lines) are collectively poorest at forecasting over this interval, suggesting that it is better to use a model derived from data directly adjacent to the forecast period, at least if the period includes a jerk. These observations are consistent with jerks being associated with a reorganization of the flow.

Maus et al. [2008] suggested that medium term (on the order of a decade) forecasts using stationary flow estimates would compensate for the effects of jerks. We have shown that this is not entirely true, since the two jerks in the decade 2000–2010 that appear to be associated with anticorrelated SA have unequal flow accelerations. Forecasts for periods soon after a jerk are best performed using steady flows and acceleration models based on data solely after the jerk epoch, if long enough (at least 3 years), or else using a steady flow if the data time span must include the jerk epoch for the flow inversion to be robust.

Figure 3 shows no discernible difference in the fit to observatory first differences data time series of the steady flow models whether they are obtained from SV data only or SV and SA data. This suggests that including the equation relating SA data to an assumed steady flow is not capturing more of the physics. Solving in addition for the steady acceleration term of the Taylor series expansion of the flow produces a small offset in the SV data predictions, to first order. Thus, the differences in the solutions arise primarily from adding in the additional time variability of the flow, rather than from including the time derivative of the

induction equation. However, even for the two types of steady flow, there are subtle differences that affect their forecasts and hindcasts.

5. Conclusions

In this paper, we described a new method for computing core flow models consisting of a steady part and its steady acceleration directly from vector SV and SA data. We calculated a series of such models from ground observatory and satellite data covering different portions of the 2000 to 2010 decade and used them to forecast and hindcast the magnetic field over the current satellite era (2000–2014.5) by advection. The RMS differences between the forecasts and the current state-of-the-art CHAOS-4+ model are always smaller for the flow and acceleration models using an appropriate data period than for similar SV forecasts from the IGRF or WMM series of models. The differences are particularly pronounced when forecasts extrapolate beyond 2010, the end of the data period considered. Jerks degrade the performance of the forecast and necessitate particular care in producing an appropriate flow model to use. Nevertheless, we suggest that core flow advection offers a useful compromise between mathematical extrapolation and complex geodynamo assimilation techniques for estimating short-term (≤ 5 years) secular variation. We recommend that such methods be incorporated into the production of future candidate reference magnetic field models, such as the next-generation IGRF.

Acknowledgments

The results presented in this paper rely on data collected at magnetic observatories. We would like to acknowledge the use of data from the CHAMP science center and the World Data Centre for Geomagnetism (Edinburgh). We thank the national institutes that support them and INTERMAGNET for promoting high standards of magnetic observatory practice (www.intermagnet.org). We also thank Susan Macmillan for preparation of the nighttime ground observatory data. We are grateful for helpful comments from reviewers Hagay Amit and Nils Olsen. This article is published with the permission of the Executive Director of the British Geological Survey (NERC).

References

- Amit, H., and P. Olson (2004), Helical core flow from geomagnetic secular variation, *Phys. Earth Planet. Inter.*, *147*, 1–25.
- Amit, H., and M. Pais (2013), Differences between tangential geostrophy and columnar flow, *Geophys. J. Int.*, *194*(1), 145–157, doi:10.1093/gji/ggt077.
- Amit, H., P. Olson, and U. Christensen (2007), Tests of core flow imaging methods with numerical dynamos, *Geophys. J. Int.*, *168*, 27–39.
- Aubert, J. (2013), Flow throughout the Earth's core inverted from geomagnetic observations and numerical dynamo models, *Geophys. J. Int.*, *192*(2), 537–556, doi:10.1093/gji/ggs051.
- Aubert, J., and A. Fournier (2011), Inferring internal properties of Earth's core dynamics and their evolution from surface observations and a numerical geodynamo model, *Nonlinear Processes Geophys.*, *18*(5), 657–674, doi:10.5194/npg-18-657-2011.
- Backus, G. E. (1968), Kinematics of geomagnetic secular variation in a perfectly conducting core, *Philos. Trans. R. Soc. London, Ser. A*, *263*, 239–266.
- Beggan, C., and K. Whaler (2008), Core flow modelling assumptions, *Phys. Earth Planet. Inter.*, *167*, 217–222.
- Beggan, C., and K. Whaler (2010), Forecasting secular variation using core flows, *Earth Planets Space*, *62*(10), 821–828, doi:10.5047/eps.2010.07.004.
- Beggan, C., K. Whaler, and S. Macmillan (2009), Temporally varying residuals of core flow models from satellite-derived 'virtual observatories', *Geophys. J. Int.*, *177*, 463–475.
- Bloxham, J. (1988), The determination of fluid flow at the core surface from geomagnetic observations, in *Mathematical Geophysics*, edited by N. J. Vlaar et al., chap. 9, pp. 189–208, D. Reidel, Dordrecht, Netherlands.
- Brown, W., J. Mound, and P. Livermore (2013), Jerks abound: An analysis of geomagnetic observatory data from 1957 to 2008, *Phys. Earth Planet. Inter.*, *223*, 62–76, doi:10.1016/j.pepi.2013.06.001.
- Chulliat, A., E. Thebaud, and G. Hulot (2010), Core field acceleration pulse as a common cause of the 2003 and 2007 geomagnetic jerks, *Geophys. Res. Lett.*, *37*, L07301, doi:10.1029/2009GL042019.
- Courillot, V., and J.-L. Le Mouél (1984), Geomagnetic secular variation impulses, *Nature*, *311*, 709–716.
- Eymin, C., and G. Hulot (2005), On core surface flows inferred from satellite magnetic data, *Phys. Earth Planet. Inter.*, *152*, 200–220, doi:10.1016/j.pepi.2005.06.009.
- Finlay, C., S. Maus, C. Beggan, M. Hamoudi, F. Lowes, N. Olsen, and E. Thébault (2010a), Evaluation of candidate geomagnetic field models for IGRF-11, *Earth Planets Space*, *62*(10), 787–804, doi:10.5047/eps.2010.11.005.
- Finlay, C. C., et al. (2010b), International Geomagnetic Reference Field: The eleventh generation, *Geophys. J. Int.*, *183*(3), 1216–1230, doi:10.1111/j.1365-246X.2010.04804.x.
- Fournier, A., J. Aubert, and E. Thébault (2011), Inference on core surface flow from observations and 3-D dynamo modelling, *Geophys. J. Int.*, *186*(1), 118–136, doi:10.1111/j.1365-246X.2011.05037.x.
- Fournier, A., L. Nerger, and J. Aubert (2013), An ensemble Kalman filter for the time-dependent analysis of the geomagnetic field, *Geochem. Geophys. Geosyst.*, *14*, 4035–4043, doi:10.1002/ggge.20252.
- Friis-Christensen, E., H. Lühr, and G. Hulot (2006), Swarm: A constellation to study the Earth's magnetic field, *Earth Planets Space*, *58*, 351–358.
- Gillet, N., M. A. Pais, and D. Jault (2009), Ensemble inversion of time-dependent core flow models, *Geochem. Geophys. Geosyst.*, *10*, Q06004, doi:10.1029/2008GC002290.
- Gubbins, D. (1982), Finding core motions from magnetic observations, *Philos. Trans. R. Soc. London, Ser. A*, *306*, 247–254.
- Gubbins, D. (1983), Geomagnetic field analysis—I. Stochastic inversion, *Geophys. J. R. Astron. Soc.*, *73*(3), 641–652.
- Gubbins, D. (1984), Geomagnetic field analysis—II. Secular variation consistent with a perfectly conducting core, *Geophys. J. Int.*, *77*(3), 753–766, doi:10.1111/j.1365-246X.1984.tb02219.
- Hamilton, B., S. Macmillan, and A. Thomson (2010), The BGS magnetic field candidate models for the 11th generation IGRF, *Earth Planets Space*, *62*(10), 737–743, doi:10.5047/eps.2010.05.005.
- Hills, R. (1979), Convection in the Earth's mantle due to viscous shear at the core-mantle interface and due to large-scale buoyancy, PhD thesis, N. M. State Univ., Las Cruces.
- Holme, R. (2007), Large-scale flow in the core, in *Treatise on Geophysics, Core Dynamics*, vol. 8, edited by P. Olson, pp. 107–130, Elsevier, Amsterdam.

- Holme, R., and O. de Viron (2013), Characterization and implications of intradecadal variations in length of day, *Nature*, *499*, 202–204, doi:10.1038/nature12282.
- Jault, D., C. Gire, and L. Le Mouél (1988), Westward drift, core motions and exchanges of angular momentum between core and mantle, *Nature*, *333*, 353–356, doi:10.1038/333353a0.
- Kahle, A., E. Vestine, and R. Ball (1967), Estimated surface motions of the Earth's core, *J. Geophys. Res.*, *72*, 1095–1108.
- Kuang, W., Z. Wei, R. Holme, and A. Tangborn (2010), Prediction of geomagnetic field with data assimilation: A candidate secular variation model for IGRF-11, *Earth Planets Space*, *62*(10), 775–785, doi:10.5047/eps.2010.07.008.
- Le Mouél, J.-L. (1984), Outer-core geostrophic flow and secular variation of Earth's geomagnetic field, *Nature*, *311*, 734–735, doi:10.1038/311734a0.
- Mandea, M., and N. Olsen (2006), A new approach to directly determine the secular variation from magnetic satellite observations, *Geophys. Res. Lett.*, *33*, L15306, doi:10.1029/2006GL026616.
- Maus, S., L. Silva, and G. Hulot (2008), Can core-surface flow models be used to improve the forecast of the Earth's main magnetic field?, *J. Geophys. Res.*, *113*, B08102, doi:10.1029/2007JB005199.
- Maus, S., S. Macmillan, S. McLean, B. Hamilton, A. Thomson, M. Nair, and C. Rollins (2010), The US/UK world magnetic model for 2010–2015, *NOAA Tech. Rep. NESDIS/NGDC*, British Geol. Surv., Boulder, Colo.
- Olsen, N., and M. Mandea (2007), Investigation of a secular variation impulse using satellite data: The 2003 geomagnetic jerk, *Earth Planet. Sci. Lett.*, *255*, 94–105.
- Olsen, N., and M. Mandea (2008), Rapidly changing flows in the Earth's core, *Nat. Geosci.*, *1*, 390–394.
- Olsen, N., M. Mandea, T. J. Sabaka, and L. Tøffner-Clausen (2009), CHAOS-2—A geomagnetic field model derived from one decade of continuous satellite data, *Geophys. J. Int.*, *179*(3), 1477–1487, doi:10.1111/j.1365-246X.2009.04386.x.
- Olsen, N., M. Mandea, T. Sabaka, and L. Tøffner-Clausen (2010), The CHAOS-3 geomagnetic field model and candidates for the 11th generation IGRF, *Earth Planets Space*, *62*, 719–727, doi:10.5047/eps.2010.07.003.
- Olsen, N., H. Lühr, C. C. Finlay, T. J. Sabaka, I. Michaelis, J. Rauberg, and L. Tøffner-Clausen (2014), The CHAOS-4 geomagnetic field model, *Geophys. J. Int.*, *197*, 815–827, doi:10.1093/gji/ggu033.
- Pais, M., and D. Jault (2008), Quasi-geostrophic flows responsible for the secular variation of the Earth's magnetic field, *Geophys. J. Int.*, *173*, 421–443, doi:10.1111/j.1365-246X.2008.03741.x.
- Rau, S., U. Christensen, A. Jackson, and J. Wicht (2000), Core flow inversion tested with numerical dynamo models, *Geophys. J. Int.*, *141*, 485–497.
- Roberts, P., and S. Scott (1965), On the analysis of the secular variation. 1. A hydromagnetic constraint: Theory, *J. Geomagn. Geoelec.*, *17*, 137–151.
- Rother, M., V. Lesur, and R. Schachtschneider (2013), An algorithm for deriving core magnetic field models from the Swarm data set, *Earth Planets Space*, *65*(11), 1223–1231, doi:10.5047/eps.2013.07.005.
- Sabaka, T. J., L. Tøffner-Clausen, and N. Olsen (2013), Use of the comprehensive inversion method for Swarm satellite data analysis, *Earth Planets Space*, *65*(11), 1201–1222, doi:10.5047/eps.2013.09.007.
- Shi, J., Z. Zhang, K. Torkar, M. Dunlop, A. Fazakerley, Z. Cheng, and Z. Liu (2014), Temporal and spatial scales of a high-flux electron disturbance in the cusp region: Cluster observations, *J. Geophys. Res. Space Physics*, *119*, 4536–4543, doi:10.1002/2013JA019560.
- Shore, R. (2013), Improved description of Earth's external magnetic fields and their source regions using satellite data, PhD thesis, Univ. Edinburgh, Edinburgh, U. K.
- Silva, L., and G. Hulot (2012), Investigating the 2003 geomagnetic jerk by simultaneous inversion of the secular variation and acceleration for both the core flow and its acceleration, *Phys. Earth Planet. Inter.*, *198–199*, 28–50, doi:10.1016/j.pepi.2012.03.002.
- Voorhies, C., and G. Backus (1985), Steady flows at the top of the core from geomagnetic field models: The steady motion theorem, *Geophys. Astrophys. Fluid Dyn.*, *32*, 163–173.
- Wahdan, A., J. Georgy, W. Abdelfatah, and A. Noureldin (2014), Magnetometer calibration for portable navigation devices in vehicles using a fast and autonomous technique, *IEEE Trans. Intell. Transp. Syst.*, *15*(5), 2347–2352, doi:10.1109/TITS.2014.2313764.
- Walker, M., and A. Jackson (2000), Robust modelling of the Earth's magnetic field, *Geophys. J. Int.*, *143*(3), 799–808.
- Wardinski, I., R. Holme, S. Asari, and M. Mandea (2008), The 2003 geomagnetic jerk and its relation to the core surface flows, *Earth Planet. Sci. Lett.*, *267*, 468–481.
- Whaler, K. (1980), Does the whole of the Earth's core convect?, *Nature*, *287*, 528–530.
- Whaler, K. A. (1986), Geomagnetic evidence for fluid upwelling at the core-mantle boundary, *Geophys. J. R. Astron. Soc.*, *86*, 563–588.